

DELAYED EMISSION FROM LUMINOUS BLUE OPTICAL TRANSIENTS IN BLACK-HOLE BINARY SYSTEMS

DAVIDE LAZZATI,<sup>1</sup> ROSALBA PERNA,<sup>2</sup> TAEHO RYU,<sup>3</sup> AND KATELYN BREIVIK<sup>4</sup>

<sup>1</sup>*Department of Physics, Oregon State University, 301 Weniger Hall, Corvallis, OR 97331, USA*

<sup>2</sup>*Department of Physics and Astronomy, Stony Brook University, Stony Brook, NY 11794-3800, USA*

<sup>3</sup>*The Max Planck Institute for Astrophysics, Karl-Schwarzschild-Str. 1, Garching, 85748, Germany*

<sup>4</sup>*McWilliams Center for Cosmology and Astrophysics, Department of Physics, Carnegie Mellon University, Pittsburgh, PA 15213, USA*

ABSTRACT

At least three members of the recently identified class of fast luminous blue optical transient show evidence of late-time electromagnetic activity in great excess of what predicted by an extrapolation of the early time emission. In particular, AT2022tsd displays fast, bright optical fluctuations approximately a month after the initial detection. Here, we propose that these transients are produced by exploding stars in black hole binary systems, and that the late-time activity is due to the accretion of clumpy ejecta onto the companion black hole. We derive the energetics and timescales involved, compute the emission spectrum, and discuss whether the ensuing emission is diffused or not in the remnant. We find that this model can explain the observed range of behaviors for reasonable ranges of the orbital separation and the ejecta velocity and clumpiness. Close separation and clumpy, high velocity ejecta result in bright variable emission, as seen in AT2022tsd. A wider separation and smaller ejecta velocity, conversely, give rise to fairly constant emission at a lower luminosity. We suggest that high-cadence, simultaneous, panchromatic monitoring of future transients should be carried out to better understand the origin of the late emission and the role of binarity in the diversity of explosive stellar transients.

*Keywords:* Binary stars – Transient sources – Supernova remnants – Black holes

1. INTRODUCTION

The last decades have seen the discovery of a variety of new transients, some of which do not immediately fit already well known phenomena. An especially interesting new class is that of the Fast Blue Optical Transients (FBOTs, e.g. Drout et al. 2014), characterized by peak luminosities  $\sim 10^{41} - 10^{44}$  erg s<sup>-1</sup>, blue colors, and rapid rises, generally < 10 days. Among these, especially interesting is the sub-class of rarer but more extremely luminous events with peak luminosities at the upper range of  $\sim 10^{44}$  erg s<sup>-1</sup>, which is often called Luminous Fast Blue Optical Transients (LFBOTs).

Unlike for ordinary supernovae (SNe), the characteristics of the LFBOTs light curves cannot be readily explained via radioactive decay of <sup>56</sup>Ni, hence requiring alternative mechanisms for powering their energetic outputs. Two broad classes of models have been proposed: those based on the interaction of an outflow with a dense circumstellar medium, which is shocked and helps convert the flow’s kinetic energy into radiation (Leung et al. 2021; Gottlieb et al. 2022; Pellegrino et al. 2022), and those based on a central engine which continues to be active for an extended period of time. Persistent sources of energy can be of different nature, from black hole (BH) accretion following the collapse of a supergiant star (Margutti et al. 2019; Perley et al. 2019; Quataert et al. 2019), to magnetars (Prentice et al. 2018; Mohan et al. 2020; Pasham et al. 2021), to BHs accreting the tidal disrupted debris of a star (Perley et al. 2019; Kuin et al. 2019). Other proposed models include the merger of a Wolf-Rayet Star with a compact object companion (Metzger 2022).

The presence of a long-lived source, while hinted in some of the FBOTS, has however been particularly evident in some of the most extreme LFBOTs, such as AT2018cow (Perley et al. 2019) and AT2022tsd (Ho et al. 2023), as well as AT2020mrf (Yao et al. 2022). In the case of At2018cow, following a steep decay of about 200 days, a low-level X-ray flux with luminosity  $\sim 10^{39}$  erg s<sup>-1</sup> was observed (Migliori et al. 2024) after more than 1000 days. Spectral analysis revealed the late emission to be of different origin than the primary one from the LFBOT. Observations with the *Hubble Space Telescope* in the UV further revealed a source of  $\sim 10^{39}$  erg s<sup>-1</sup> at 703 days and at 1453 days (Chen

et al. 2023), with a mild decay between the two epochs, which argued against being a stable background, but rather a late-time association to AT2018cow.

The transient AT2020mrf (Yao et al. 2022) had an optical spectrum displaying a strong resemblance to the one of AT2018cow. Likewise this transient, it was observed to exhibit late-time X-ray emission, albeit more than 200 times more intense than for the AT2018cow. In particular, at 328 days after its start, the *Chandra* telescope detected the source at a level of  $L_X \sim 10^{42}$  erg s $^{-1}$ . The emission was found to be variable on a timescale of  $\sim 1$  day.

The AT2022tsd transient has similar evidence for the presence of a long-lasting, possibly distinct secondary emission component. Starting at about 26 days after the initial discovery, optical photometry revealed flaring activity, persisting for about 100 days and with intensity nearly comparable to that of the original transient,  $\sim 10^{44}$  erg s $^{-1}$  (Ho et al. 2023).

The presence of a secondary, persistent energy source places further constraints on models for LFBOTs. Here we argue that, in LFBOT models in which the primary emission is produced as a result of a SN explosion, the extended emission can be reproduced if the newly formed BH (or magnetar) has a BH companion formed from a former SN explosion which did not unbind the binary.

This fraction of survived binaries has been studied both relying on observations (e.g., Kochanek 2021; Neustadt et al. 2021; Byrne & Fraser 2022), as well as by adopting population synthesis models (e.g. Kochanek et al. 2019). It was found to range between a few percent and several tens of percent.

Our model relies on a naturally occurring phenomenon connected to the second SN explosion: the interaction of the SN ejecta with the remnant BH of the primary star. The possibility of electromagnetic emission from the birth of binary BHs was previously discussed by Kimura et al. (2017a) and Kimura et al. (2017b). They studied outflow-driven transients in tidally-locked SNe where the progenitor binary is made up of a Wolf-Rayet star and a BH. When the second star goes off as a SN, some of the material is gravitationally captured by the primary BH, forming an accretion disk and driving a powerful wind. The energy of the wind, in turn, is deposited in the rest of the ejecta, and radiation diffusively emerges. Another binary-driven emission scenario was proposed by Fryer et al. (2014) as a gamma-ray burst (GRB) model: ejecta from the explosion of a SN rapidly accrete onto a neutron star companion, causing it to collapse onto a BH. The hyperaccreting conditions of the induced gravitational collapse would lead to a GRB-like transient.

Here we specifically focus on the LFBOT late-time emission, which in at least some cases follows after a period of quietness. We suggest that it is the result of accretion of clumpy ejecta from the SN of the secondary star onto the primary BH. Unlike traditional models in which the late emission is produced by the same primary engine, a quiescent phase is naturally predicted in the case of an accreting companion, correlating with the time that the SN ejecta take to travel from the exploding star to the BH companion. Additionally, the optical depth of the ejecta surrounding the companion is expected to be smaller than if the central engine were located at the center of the SN.

We specifically focus on a scenario in which the SN ejecta are inhomogeneous, as found both from SN observations (Fransson & Chevalier 1989; Jerkstrand et al. 2011; Abellán et al. 2017), as well as theoretical models (Wang & Chevalier 2002; Wang 2001; Dessart et al. 2018). In this case, the resulting accretion is expected to be episodic, possibly producing flare-like emission. As quantified in this work, the observable properties of these transients will mainly depend on the ejecta properties, such as its mass, velocity, clumping fraction, as well as the orbital separation and mass of the BH companion.

This paper is organized as follows: first we summarize the observations, with special emphasis on the late emission of the three sources we study (Sec. 2); we then present our analytic model for late emission due to accretion of ejecta clumps onto the black hole companion (Sec. 3), discussing in detail the expected accretion rates (Sec. 3.1), the emission mechanisms (Sec. 3.2), and the opacity encountered by the escaping radiation (Sec. 3.3). In Sec. 4, we perform population synthesis calculations aimed at testing the likelihood of our inferred binary parameters. We summarize and conclude in Sec. 5.

## 2. DELAYED EMISSION FROM THE TRANSIENTS AT2018COW, AT2020MRF, AT2022TSD

In the following we summarize the main observations of the three FBOTs which are known to display late-time emission.

### 2.1. AT2018cow

AT2018cow is a relatively nearby FBOT, exploded on 16 June 2018 at a distance of  $\sim 62$  Mpc in a star-forming dwarf galaxy (Prentice et al. 2018). Initially detected in optical (Smartt et al. 2018), it reached a peak luminosity of

$\sim 4 \times 10^{44}$  erg/s (Margutti et al. 2019) and it was detected over a wide electromagnetic range, from hard X-rays at energies  $> 10$  keV, to the radio band. The latter was found consistent with the interaction of a blast wave of  $v \sim 0.1c$  with a dense environment (Margutti et al. 2019). However, a search for  $\gamma$ -ray emission with the Inter-Planetary network ruled out emission with peak luminosity  $> 10^{47}$  erg/s, hence further differentiating this transient from a standard gamma-ray burst.

After its discovery, AT2018cow was continued to be monitored. Its luminosity was found to have considerably dropped, by about 4 orders of magnitude down to  $2 \sim 10^{39}$  erg/s, after about 200 days from the initial discovery (Migliori et al. 2024). However, an X-ray source at a level lower by only a factor  $\lesssim 4$  was still present after about 3.7 years (Migliori et al. 2024). Multiband UV photometry acquired with the Hubble telescope at around the same time at the location of AT2018cow revealed the presence of a source with luminosity  $L_{UV} \sim 10^{39}$  erg/s (Chen et al. 2023). The UV spectrum was found to be consistent with the Rayleigh-Jeans tail of a thermal spectrum with effective temperature  $T_{\text{eff}} \gtrsim 10^{4.6}$  K. Considering the possibility that the optical, UV and X-ray emission come from the same origin, Margutti et al. (2019) fitted it with a Shakura & Sunyaev (1973) multibody disk with inner temperature of  $T_{\text{in}} \sim 10^{5.91}$  K and outer temperature  $T_{\text{out}} \sim 10^{4.45}$  K.

While the observed late emission could be interpreted within the context of an accretion disk around an intermediate mass BH (Migliori et al. 2024), in the following we will entertain the possibility that it is the result of accretion onto a companion BH, motivated by the observation that the late-time emission appears of a different nature than the one of the main LFBOT (Migliori et al. 2024).

## 2.2. AT2020mrf

The FBOT AT2020mrf was discovered on 12 June 2020 by ZTF. Its X-ray, optical and radio properties were reported by Yao et al. (2022), together with the analysis of the host galaxy. Likewise for the AT2018cow, the host was found to be a dwarf galaxy; its mass was estimated to be  $M_* \sim 10^8 M_\odot$ , and its specific star formation rate  $\sim 10^{-1}$  yr $^{-1}$ . The metallicity of the galaxy was estimated between  $10^{-0.70} - 10^{-0.13} Z_\odot$ . The optical spectrum of the transient was fitted by a blackbody with temperature  $T \sim 2 \times 10^4$  K and emitting radius  $R \sim 8 \times 10^{14}$  cm. The X-ray luminosity, on the order of  $2 \times 10^{43}$  erg/s at  $\sim 36$  days, is comparable to that of cosmological GRBs. However, the  $\gamma$ -ray upper limit of  $\sim 10^{49}$  erg/s from Konus-Wind is considerably lower than that of a standard GRB seen on-axis. The bright radio luminosity, at a level of  $\sim 10^{39}$  erg/s, could be explained as synchrotron emission from the interaction between a blastwave with velocity  $v \sim 0.07 - 0.08 c$  and a dense medium, similarly to AT2018cow.

The source At2020mrf was again detected in X-rays by *Chandra* at 328 days, with a luminosity level of  $\sim 10^{42}$  erg/s and with intraday variability (Yao et al. 2022). This emission was found to be too bright to be an extension of the radio synchrotron spectrum. The spectrum at 328 days was found to be harder,  $F_\nu \propto \nu^0$  compared to the spectrum at  $\sim 36$  days,  $F_\nu \propto \nu^{-0.8}$ .

Similarly to the case of AT2018cow, the properties of AT2020mrf require an extended energy source, for whom the most natural candidates are either a magnetar or an accreting BH. If the FBOT is produced by the result of a successful SN-like explosion, then no significant emission from fallback is expected at about a year (e.g. Zhang et al. 2008; Perna et al. 2014), while a failed explosion would require a weakly bound red giant progenitor (Yao et al. 2022). In the case of a remnant magnetar, X-rays may be generated at the termination shock of a pulsar wind nebula (Lyutikov 2022). In the following we will show that the late emission of AT2020mrf can be naturally explained within our scenario.

## 2.3. AT2022tsd

AT2022tsd, also known as the Tasmanian Devil, was discovered on 7 September 2022 by the Zwicky Transient Facility, and was promptly followed with an array of telescopes, revealing the source across a broad electromagnetic spectrum from the X-rays to the millimeter (Ho et al. 2023). It was localized at about 6 kpc from the center of a dwarf galaxy.

The presence of a long-lived energy source is particularly evident for this transient. Starting at about 26 days after the initial transient discovery, optical photometry revealed flaring activity, persisting for about 100 days. A total of 14 flares were recorded, with minute-timescale duration, and occasional luminosity that was nearly as bright as that of the original transient,  $\sim 10^{44}$  erg s $^{-1}$ . Additionally, in between flares, flux variations exceeding an order of magnitude on timescales shorter than 20 s were also observed.

The flare analysis performed by Ho et al. (2023) revealed a radius of the emitting region which is much smaller than the blackbody radius of the early emission from the LFBOT. The short timescales of the flares, combined with

Physical parameter	symbol	fiducial value
orbital diameter	$d$	10 AU
velocity of the SN ejecta	$v_{\text{ej}}$	$10^8 \text{ cm s}^{-1}$
mass of the companion BH	$M_{\text{BH}}$	$15 M_{\odot}$
mass of the SN ejecta	$M_{\text{ej}}$	$1 M_{\odot}$
thickness of the ejecta	$\Delta$	$d$
volume filling factor of ejecta clumps	$\zeta$	$10^{-3}$
clump radius relative to ejecta	$\xi$	$10^{-3}$
BH ejection efficiency	$\eta$	0.1
Impact parameter of individual clump	$r_0$	$4 \times 10^{11} \text{ cm}$

**Table 1.** Physical parameters of the model and their fiducial values used for order of magnitude estimates.

their large energetics, imply optically thin emission from an at least mildly relativistic outflow with velocity  $v/c \gtrsim 0.6$ . Therefore, they conclude that there must be a long-lived engine associated with the initial FLBOT transient. As will be shown in the following, the model proposed here provides a compelling explanation for the origin of these observed flares.

### 3. LATE EMISSION FROM CLUMPY ACCRETION ONTO A BH COMPANION

#### 3.1. Mass inflow

Let us consider a binary system with separation  $d$ . The system contains an evolved star that has recently exploded as a core-collapse SN, and a companion BH. The exploded star has ejected a mass  $M_{\text{ej}}$  at a velocity  $v_{\text{ej}}$ <sup>1</sup> (see a graphical representation of this scenario in Figure 1, and also [Kimura et al. 2017a,b](#) for a similar scenario). For the case of uniform ejecta we follow closely the derivation in [Kimura et al. \(2017b\)](#). We then extend the formalism by considering clumping of the ejecta. The ejecta reach the BH after a time

$$\Delta t_{\text{SN-trans}} = \frac{d}{v_{\text{ej}}} = 17 \left( \frac{d}{10 \text{ AU}} \right) \left( \frac{v_{\text{ej}}}{10^8 \frac{\text{cm}}{\text{s}}} \right)^{-1} \text{ d}. \quad (1)$$

Since the ejecta velocity is likely to greatly exceed their sound speed, the cross section for accretion onto the companion BH is given by the Hoyle-Littleton radius (e.g., [Edgar 2004](#)):

$$r_{\text{acc}} = \frac{2GM_{\text{BH}}}{v_{\text{ej}}^2} = 4 \times 10^{11} \left( \frac{M_{\text{BH}}}{15M_{\odot}} \right) \left( \frac{v_{\text{ej}}}{10^8 \frac{\text{cm}}{\text{s}}} \right)^{-2} \text{ cm}, \quad (2)$$

where  $M_{\text{BH}}$  is the mass of the BH. The total accreted mass after the entire remnant has crossed the BH orbit is therefore:

$$M_{\text{acc}} = M_{\text{ej}} \frac{r_{\text{acc}}^2}{4d^2} = M_{\text{ej}} \frac{(GM_{\text{BH}})^2}{d^2 v_{\text{ej}}^4} = 1.8 \times 10^{-6} \left( \frac{M_{\text{ej}}}{M_{\odot}} \right) \left( \frac{M_{\text{BH}}}{15M_{\odot}} \right)^2 \left( \frac{d}{10 \text{ AU}} \right)^{-2} \left( \frac{v_{\text{ej}}}{10^8 \frac{\text{cm}}{\text{s}}} \right)^{-4} M_{\odot}. \quad (3)$$

If we consider a remnant with radial thickness  $\Delta$ , an estimate of the average accretion rate yields

$$\dot{M}_{\text{acc}} = \frac{M_{\text{acc}} v_{\text{ej}}}{\Delta} = M_{\text{ej}} \frac{(GM_{\text{BH}})^2}{d^2 \Delta v_{\text{ej}}^3} = 10^{-12} \frac{d}{\Delta} \left( \frac{M_{\text{ej}}}{M_{\odot}} \right) \left( \frac{M_{\text{BH}}}{15M_{\odot}} \right)^2 \left( \frac{d}{10 \text{ AU}} \right)^{-3} \left( \frac{v_{\text{ej}}}{10^8 \frac{\text{cm}}{\text{s}}} \right)^{-3} \frac{M_{\odot}}{\text{s}}. \quad (4)$$

We note that this rate is highly super-Eddington, the Eddington accretion rate onto a  $15 M_{\odot}$  black hole being  $\sim 10^{-15}/\eta (M_{\odot}/\text{s})$ , where  $\eta$  represents an efficiency for the conversion of accreted rest-mass  $\dot{M}_{\text{acc}} c^2$  into radiated luminosity. The inflow is also likely to form an accretion disk because of the orbital angular momentum ([de Val-Borro et al. 2009](#); [Huarte-Espinosa et al. 2013](#)). Accretion disks onto BHs with super-Eddington accretion rates are known, from both theoretical investigations (e.g. [Blandford & Begelman 1999](#)), numerical simulations (e.g. [Takeuchi et al.](#)

<sup>1</sup> Most likely the ejecta have a spread of velocities. See the discussion for an evaluation of the impact of such occurrence.

2013; Jiang et al. 2014), and observations (e.g. Fabrika 2004) to feature strong outflows. If we make this assumption here, and indicate with  $\Omega$  the outflow collimation angle, we obtain an average observed bolometric luminosity:

$$\bar{L}_{\text{iso}} = \eta \frac{4\pi}{\Omega} \bar{M}_{\text{acc}} c^2 \simeq 2 \times 10^{42} \eta \frac{4\pi}{\Omega} \frac{d}{\Delta} \left( \frac{M_{\text{ej}}}{M_{\odot}} \right) \left( \frac{M_{\text{BH}}}{15M_{\odot}} \right)^2 \left( \frac{d}{10 \text{ AU}} \right)^{-3} \left( \frac{v_{\text{ej}}}{10^8 \frac{\text{cm}}{\text{s}}} \right)^{-3} \frac{\text{erg}}{\text{s}}, \quad (5)$$

which is a considerable energy output, comparable to the supernova luminosity at peak.

As discussed above, a more accurate model would be one in which the SN ejecta are clumped, characterized by a clump volume filling factor  $\zeta$  and by a typical clump radius  $r_c = \xi d$ . In this case, the emitted power is more accurately calculated as the mass of a single clump over the time it takes for the clump to be accreted via a disk by the central black hole, modified with the efficiency and geometric beaming factors as above. We now explore this scenario in more detail.

The total number of clumps in the remnant is given by

$$N_c = \frac{3d^2\Delta}{r_c^3} \zeta = 3 \frac{\zeta}{\xi^3} \frac{\Delta}{d} = 3 \times 10^6 \frac{\Delta}{d} \left( \frac{\zeta}{10^{-3}} \right) \left( \frac{\xi}{10^{-3}} \right)^{-3}, \quad (6)$$

where the fiducial values for  $\zeta$  and  $\xi$  are taken from both observational (e.g. Fransson & Chevalier 1989) and theoretical (e.g. Dessart et al. 2018) studies. Of all such clumps, the number of those that fall within the BH accretion radius reads:

$$N_{\text{acc}} = \frac{\pi r_{\text{acc}}^2}{4\pi d^2} N_c = 3 \left( \frac{GM_{\text{BH}}}{d v_{\text{ej}}^2} \right)^2 \frac{\zeta}{\xi^3} \frac{\Delta}{d} = 5 \frac{\Delta}{d} \left( \frac{M_{\text{BH}}}{15M_{\odot}} \right)^2 \left( \frac{d}{10 \text{ AU}} \right)^{-2} \left( \frac{v_{\text{ej}}}{10^8 \frac{\text{cm}}{\text{s}}} \right)^{-4} \left( \frac{\zeta}{10^{-3}} \right) \left( \frac{\xi}{10^{-3}} \right)^{-3}. \quad (7)$$

Clump accretion can take place under two distinct regimes, depending on the system properties. For small orbital separation, it is likely that the clumps are smaller than the accretion radius in Eq. 2, while at larger separations partial accretion of big clumps would be possible. The orbital separation at which large clump accretion becomes relevant is

$$d > 2 \frac{GM_{\text{BH}}}{\xi v_{\text{ej}}^2} = 26 \left( \frac{M_{\text{BH}}}{15M_{\odot}} \right) \left( \frac{\xi}{10^{-3}} \right)^{-1} \left( \frac{v_{\text{ej}}}{10^8 \frac{\text{cm}}{\text{s}}} \right)^{-2} \text{ AU}. \quad (8)$$

We note that if Eq. 8 is satisfied, then the number of accreted clumps falls below unity (see Eq. 7) and we therefore concentrate on the small clumps regime. At large radii, the accretion is likely to be dominated by the intra-clump ejecta, following Eqs. 4 and 5.

Let us consider a small clump approaching the accretion region with an impact parameter  $r_0$  (so  $r_0 \lesssim r_{\text{acc}}$ ) around the BH and with velocity  $v_{\text{ej}}$ . When a clump enters the Hoyle-Littleton sphere of the BH, the clump falls towards the BH on the free-fall timescale:

$$t_{\text{ff}} \approx \sqrt{\frac{r_{\text{acc}}^3}{GM_{\text{BH}}}} = 2\sqrt{2} \frac{GM_{\text{BH}}}{v_{\text{ej}}^3} \simeq 1.5 \left( \frac{M_{\text{BH}}}{15M_{\odot}} \right) \left( \frac{v_{\text{ej}}}{10^8 \frac{\text{cm}}{\text{s}}} \right)^{-3} \text{ hour}. \quad (9)$$

If the angular momentum loss is negligible in its decaying orbit, the clump would circularize (once shredded as a result of tidal forces and pressure gradients during the infall towards the BH) at a radius  $r_{\text{circ}}$  at which its specific angular momentum equals the one of a Keplerian orbit, or  $r_0 v_{\text{ej}} \sim r_{\text{circ}} \sqrt{GM_{\text{BH}}/r_{\text{circ}}}$ . This relation yields:

$$r_{\text{circ}} = \frac{r_0^2 v_{\text{ej}}^2}{GM_{\text{BH}}} = 2 \times 10^{11} \left( \frac{M_{\text{BH}}}{15M_{\odot}} \right)^{-1} \left( \frac{r_0}{4 \times 10^{11} \text{ cm}} \right)^2 \left( \frac{v_{\text{ej}}}{10^8 \frac{\text{cm}}{\text{s}}} \right)^2 \text{ cm}. \quad (10)$$

Note that in realistic situations, infalling streams are bent around the BH and collide with each other, resulting in deflecting some of the streams towards the BH. For such cases, the circularization radius would be smaller than our crude estimate of  $r_{\text{circ}}$ . In this sense,  $r_{\text{circ}}$  in Equation 10 should be considered as an upper limit. Lower values would yield shorter timescales for accretion and hence higher peak luminosities (see below).

Upon circularization, the material will accrete onto the BH on the viscous timescale, which reads (for a puffy disk, as typical of hyperaccretion):

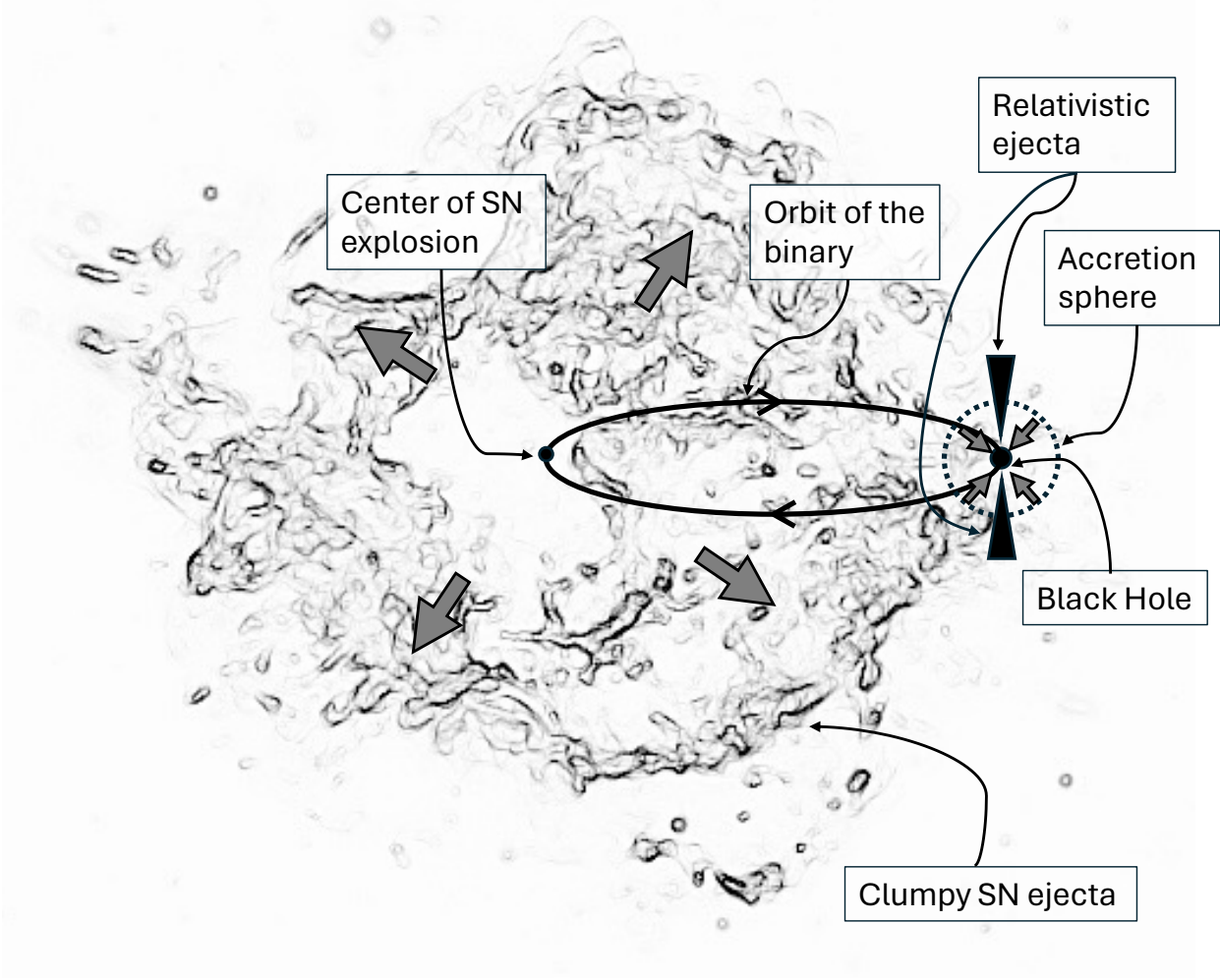


**Figure 1.** Cartoon of the post SN explosion binary system, as envisioned in this model. The SN ejecta have expanded to reach the orbit of the companion BH, which is accreting mass via the Hoyle-Littleton mechanism. Ejecta clumps are shredded into an accretion disk and the accreting BH is ejecting a collimated relativistic outflow that is eventually responsible for the observed non-thermal electromagnetic emission.

$$t_{\text{visc}} \simeq \frac{1}{\alpha} \left( \frac{r_{\text{circ}}^3}{GM_{\text{BH}}} \right)^{1/2} = \frac{1}{\alpha} \frac{(r_0 v_{\text{ej}})^3}{(GM_{\text{BH}})^2} \simeq 1.5 \times 10^5 \left( \frac{\alpha}{0.1} \right)^{-1} \left( \frac{M_{\text{BH}}}{15M_{\odot}} \right)^{-2} \left( \frac{r_0}{4 \times 10^{11} \text{cm}} \right)^3 \left( \frac{v_{\text{ej}}}{10^8 \frac{\text{cm}}{\text{s}}} \right)^3 \text{ s}, \quad (11)$$

where  $\alpha$  is the viscosity parameter (Shakura & Sunyaev 1973). The clump accretion rate may thus be estimated as

$$\begin{aligned} \dot{M}_c &\simeq \frac{M_c}{t_{\text{visc}}} = \frac{\alpha}{3} \frac{d}{\Delta} \frac{\xi^3}{\zeta} G^2 \frac{M_{\text{ej}} M_{\text{BH}}^2}{r_0^3 v_{\text{ej}}^3} \\ &\simeq 2 \times 10^{-12} \frac{d}{\Delta} \left( \frac{\alpha}{0.1} \right) \left( \frac{\xi}{10^{-3}} \right)^3 \left( \frac{\zeta}{10^{-3}} \right)^{-1} \left( \frac{M_{\text{ej}}}{1 M_{\odot}} \right) \left( \frac{M_{\text{BH}}}{15 M_{\odot}} \right)^2 \left( \frac{r_0}{4 \times 10^{11} \text{cm}} \right)^{-3} \left( \frac{v_{\text{ej}}}{10^8 \frac{\text{cm}}{\text{s}}} \right)^{-3} \frac{M_{\odot}}{\text{s}}, \quad (12) \end{aligned}$$

where we have estimated the clump mass as  $M_c = M_{\text{ej}}/N_c$ , which is valid if the clumps carry the majority of the ejecta mass. Note that the viscous time and, consequently, the accretion rate have a strong dependence on the impact parameter  $r_0$  and ejecta velocity  $v_{\text{ej}}$ . For a given ejecta velocity, the accretion rate of the clumps with small impact parameter  $r_0$  is going to be much higher than the one of the — far more numerous — clumps that are accreted with

an impact parameter comparable to the BH accretion radius  $r_{\text{acc}}$ . The accretion rate history of the BH is therefore characterized by a low-level steady state from the tenuous intra-cluster ejecta material, numerous long-lasting low-level events from clumps accreted with  $r_0 \sim r_{\text{acc}}$ , and few strong events when a low impact parameter clump is accreted.

To evaluate the maximum expected accretion rate, we consider that the clump with the smallest impact parameter has  $r_0 \sim r_c$ . In addition, we calculate the number of clumps that are expected to accrete with an impact parameter compared to their size to be:

$$N_{c,r_0=r_c} = N_c \frac{\pi r_c^2}{4\pi d^2} = \frac{3}{4} \frac{\zeta}{\xi} \frac{\Delta}{d}, \quad (13)$$

which is of order unity for the fiducial model parameters described in Table 1. The maximum expected accretion rate (Eq 12 at  $r_0 = r_c$ ) is therefore:

$$\dot{M}_{\text{max}} = \frac{\alpha}{3\zeta} \frac{d}{\Delta} G^2 \frac{M_{\text{ej}} M_{\text{BH}}^2}{d^3 v_{\text{ej}}^3} = 4 \times 10^{-11} \frac{d}{\Delta} \left(\frac{\alpha}{0.1}\right) \left(\frac{\zeta}{10^{-3}}\right)^{-1} \left(\frac{M_{\text{ej}}}{1 M_{\odot}}\right) \left(\frac{M_{\text{BH}}}{15 M_{\odot}}\right)^2 \left(\frac{d}{10 \text{ AU}}\right)^{-3} \left(\frac{v_{\text{ej}}}{10^8 \frac{\text{cm}}{\text{s}}}\right)^{-3} \frac{M_{\odot}}{\text{s}}. \quad (14)$$

As mentioned above, given the highly super-Eddington accretion rates, and the suitable conditions for circularization of the clump ejecta, it is presumable that a beamed and moderately relativistic outflow may be launched (e.g., Blandford & Znajek 1977; Tchekhovskoy et al. 2011; Qian et al. 2018; Parfrey et al. 2019). Let its opening angle be  $\Omega$ . We can then estimate the isotropic equivalent kinetic energy that is ejected from the BH as a result of the accretion of a clump, which can be potentially radiated as an electromagnetic transient:

$$L_{c,\text{iso}} = \eta \frac{4\pi}{\Omega} \dot{M}_c c^2 \simeq 3 \times 10^{42} \eta \frac{4\pi}{\Omega} \frac{d}{\Delta} \left(\frac{\alpha}{0.1}\right) \left(\frac{\xi}{10^{-3}}\right)^3 \left(\frac{\zeta}{10^{-3}}\right)^{-1} \left(\frac{M_{\text{ej}}}{1 M_{\odot}}\right) \left(\frac{M_{\text{BH}}}{15 M_{\odot}}\right)^2 \left(\frac{r_0}{4 \times 10^{11} \text{ cm}}\right)^{-3} \left(\frac{v_{\text{ej}}}{10^8 \frac{\text{cm}}{\text{s}}}\right)^{-3} \frac{\text{erg}}{\text{s}}. \quad (15)$$

The maximum luminosity is correspondingly given by

$$L_{\text{max,iso}} = \eta \frac{4\pi}{\Omega} \dot{M}_{\text{max}} c^2 \simeq 7 \times 10^{43} \eta \frac{4\pi}{\Omega} \frac{d}{\Delta} \left(\frac{\alpha}{0.1}\right) \left(\frac{\zeta}{10^{-3}}\right)^{-1} \left(\frac{M_{\text{ej}}}{1 M_{\odot}}\right) \left(\frac{M_{\text{BH}}}{15 M_{\odot}}\right)^2 \left(\frac{d}{10 \text{ AU}}\right)^{-3} \left(\frac{v_{\text{ej}}}{10^8 \frac{\text{cm}}{\text{s}}}\right)^{-3} \frac{\text{erg}}{\text{s}}. \quad (16)$$

If we now substitute the clump radius in Eq. 11, we obtain the minimum variability timescale, which is associated with the brightest flares, as:

$$t_{\text{var, min}} = \frac{1}{\alpha} \frac{(\xi d v_{\text{ej}})^3}{(GM_{\text{BH}})^2} = 2 \left(\frac{\alpha}{0.1}\right)^{-1} \left(\frac{\xi}{10^{-3}}\right)^3 \left(\frac{d}{10 \text{ AU}}\right)^3 \left(\frac{v_{\text{ej}}}{10^8 \frac{\text{cm}}{\text{s}}}\right)^3 \left(\frac{M_{\text{BH}}}{15 M_{\odot}}\right)^{-2} \text{ h}. \quad (17)$$

We notice that the maximum luminosity in Eq. 16 scales with the binary properties analogously to the average luminosity in Eq. 5, so that we can write:

$$L_{\text{max,iso}} = \frac{\alpha}{3\zeta} \frac{d}{\Delta} \bar{L}_{\text{iso}} \simeq 33 \left(\frac{\alpha}{0.1}\right) \left(\frac{\zeta}{10^{-3}}\right)^{-1} \frac{d}{\Delta} \bar{L}_{\text{iso}}. \quad (18)$$

Fig. 2 shows, for the fiducial parameters in Table 1, how the delay and the luminosity of the accreting primary BH vary as a function of the binary BH orbital distance and the velocity of the SN ejecta. Note the degeneracy between these two variables both in reproducing a luminosity value as well as a time delay. However, the different functional form of the correlation allows one to identify specific regions in the  $\{d, v_{\text{ej}}\}$  parameter space when observations provide constraints on both luminosity and time delay.

The vertical line in the figure separates the region to the left, where individual clumps dominate, and hence flaring emission is more likely expected with the enhanced luminosity of Eq. 16, from the region to the right, where the emission is more likely to be continuous and hence the luminosity is expected to be closer to the average value of Eq. 5. The location of the line is set by Eq. 8.

Last, the gray area in the upper left corner indicates a region in which transients from the accreting companion BH would likely be outshined by (or at least confused with) the primary emission from the FBOT itself. This has been taken corresponding to a time delay between the FBOT and the later emission of  $\leq 2$  weeks.

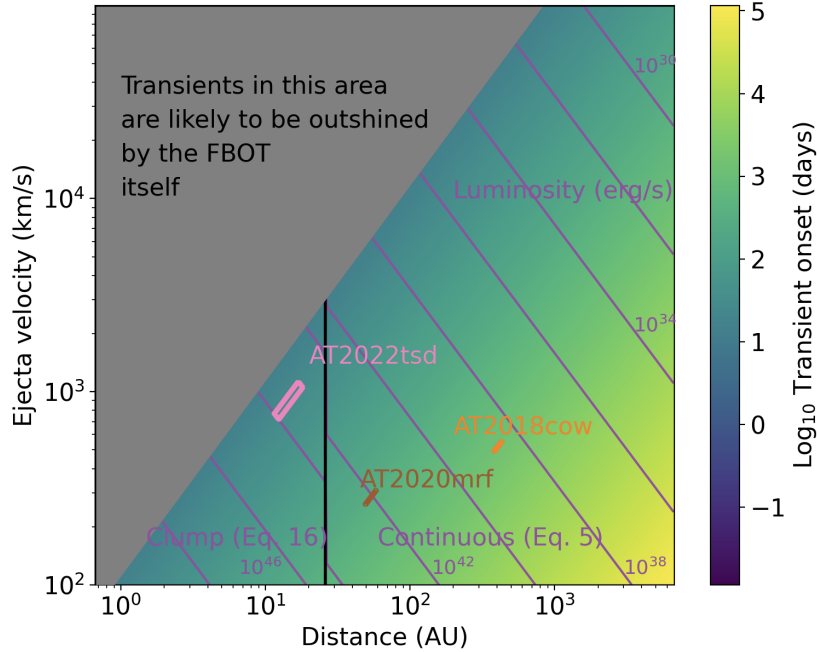


**Figure 2.** Delay and luminosity of the BH-powered transients from accretion induced by a supernova in the binary system as a function of the binary separation and the ejecta velocity. Time delay is shown in pseudocolors (see colorbar), while average luminosity from Eqs. 5 and 16 is shown with contour levels. A vertical black line separates the region in which accretion from individual clumps dominates (left, Eq. 16) and the region in which accretion is dominated by the intraclump medium. The location in the parameter space of the late emission from the three considered FBOTs is also shown. Except from binary separation  $d$  and ejecta velocity  $v_{ej}$ , all parameters are set to their fiducial values shown in Table 1.

Examining more in detail Fig. 2 for each of the sources, we see that, for the case of AT2018cow, a luminosity on the order of  $\sim 10^{39}$  erg/s with a time delay of 3.7 years can be produced with a BH companion at a distance of about 400 AU, accreting SN ejecta moving at a speed of  $\sim 500$  km/s. For this parameter set, accretion is dominated by the intra-clump medium (cfr. Eq. 8), and pronounced variability is not expected. The case of AT2018cow is, however, unique among the FLBOTs discussed here since excess X-ray emission has been detected at multiple times with no indication of fast variability. If, for example, the component seen at 220 days is interpreted as the beginning of the accretion phase onto the companion BH, then the point corresponding to AT2018cow in Fig. 2 would move along a track parallel to the blue lines, to an orbital distance of about 100 AU and an ejecta velocity of about  $2 \times 10^3$  km/s. Either way, the region in the parameter space would correspond to one in which the emission is not expected to display flaring due to clumps (consistent with observations). We also note that our inferred ejecta speeds, when combined with the blastwave velocity of  $\sim 0.1c$  required to explain the early radio emission from the FBOT (Margutti et al. 2019), would indicate an asymmetric SN explosion and/or that the mildly relativistic component whose interaction with the dense medium produces the FBOT radio emission is powered by the outflow/jet which emerges perpendicularly to the orbital plane, where the slower SN ejecta move.

For the case of AT2020mrf, the detected emission at 326 days with a luminosity of  $\sim 10^{42}$  erg/s places the accreting BH companion at an orbital distance of about 50 AU and ejecta speed of about 400 km/s. However, we note that the extended X-ray component could have started earlier, any time between 36-days - 336 days, when there were no observations. This would move the point in Fig. 2 along the blue line corresponding to  $10^{42}$  erg/s, reaching at  $t = 75$  d the border with the region where variable, late-emission is expected.

Last, as shown in Fig. 2 for the source AT2022tsd, for our fiducial choices of BH companion mass and SN ejecta properties, the flare luminosity of  $\sim 10^{44}$  erg s $^{-1}$ , and the  $\sim 1$  month delay of the late emission can be reproduced for a BH binary with an orbital separation of  $\sim 15$  AU and ejecta velocity  $\sim 10^3$  km/s.

Taking this parameter set at face value, Eq. 17 gives a variability timescale of several hours, in excess of the observed timescale of tens of minutes. This tension between the model and the observations can be easily ameliorated by slightly modifying the adopted fiducial model parameters, such as increasing the accreting BH mass or decreasing the size of



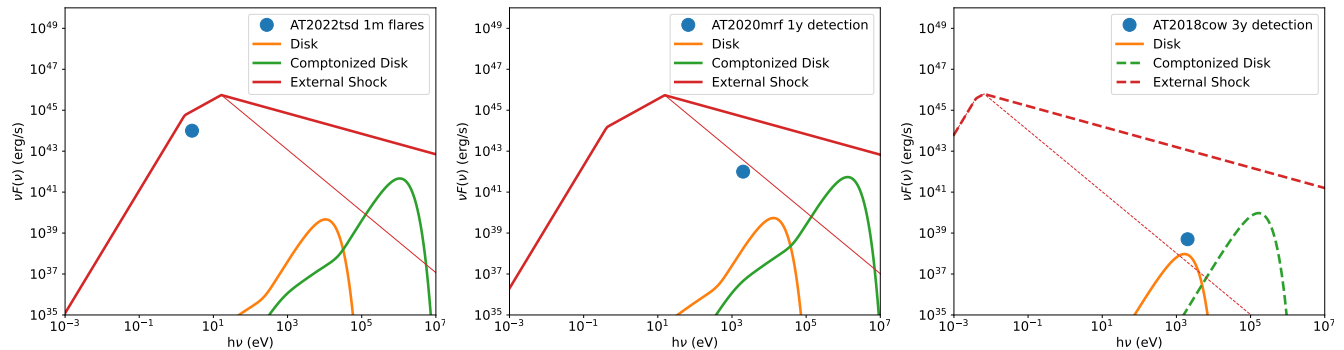


**Figure 3.** Various components of the emission spectrum of a BH accreting from SN ejecta: an accretion disk, Comptonized disk emission, and radiation from an external shock formed from the interaction of an accretion-driven outflow with the dense SN medium. Dashed lines are used to emphasize that an accretion-driven outflow might not form when the accretion is sub-Eddington. A thin line is used, instead, for the high-frequency slope of the external shock component in case of a steeper electron distribution. For each source, the model parameters are varied to produce the best match to the late-time observations (see text).

the clumps. For example, reducing by a factor 3 the clumping factor to  $\xi = 3 \times 10^{-4}$  (with all the other parameters remaining the same), would yield a variability timescale of  $\sim 15$  minutes. In addition, instabilities in the accretion and/or substructure in the clumps geometry would result in variable luminosity on shorter timescales than the order of magnitude estimate provided by Eq. 17.

We finally note that, in all the cases, the inferred ejecta velocities are on the lower end for core-collapse supernovae. However, in our model the companion BH receives the equatorial ejecta from the exploding star, while the supernova itself is likely observed from the polar direction. If FLBOTs are engine driven, as suggested by numerous models (e.g., Margutti et al. 2019; Perley et al. 2019), a polar dependence of the supernova ejecta is to be expected. In addition, the emission from the companion BH is likely to be dominated by slower ejecta (Eq. 16), which carry more mass than the ejecta that are in the leading edge of a homologous expansion (see, e.g., Chevalier & Soker 1989; Lazzati et al. 2012).

### 3.2. Electromagnetic emission

Let us now consider the electromagnetic signal that is produced by the accreting companion BH. Since the accreting material forms a disk, we first consider the emission coming from the disk itself. Accretion rates are in most cases highly super-Eddington, therefore we compute the disk emission using the effective temperature profile derived for hyper-accreting conditions (Kawaguchi 2003):

$$T_{\text{eff}}(r) = 1.8 \times 10^8 \left( \frac{M_{\text{BH}}}{15M_{\odot}} \right)^{-1/4} \left( \frac{\dot{M}_{\text{acc}} c^2}{10^4 L_{\text{Edd}}} \right)^{1/4} \left( \frac{R}{R_{\text{Sch}}} \right)^{-3/4} \left( 1 - \sqrt{\frac{3R_{\text{Sch}}}{R}} \right)^{1/4} \text{ K}, \quad (19)$$

where  $R_{\text{Sch}}$  is the Schwarzschild radius, and where the inner and outer disk radii are assumed to be  $3R_{\text{Sch}}$  and the circularization radius of Eq. 10, respectively. The emission spectrum is computed by integrating over radius, assuming local black body properties. The overall spectrum is then normalized to the luminosity values reported in Kawaguchi (2003) (see their Figure 12), who properly take into account the effect of opacity and relativistic redshift in their calculations. This component is shown in Figure 3 with a solid orange line. We notice, in addition, that the disk would likely eject also a subrelativistic wind, especially if the mass inflow rate is super-Eddington (e.g., Blandford & Begelman 1999). If this wind is optically thick, the disk radiation would be reprocessed in the wind. As a consequence, it would be converted to shorter wavelengths and the total energetics decreased due to adiabatic losses (Piro & Lu 2020).

In addition to the disk emission, a collimated relativistic outflow is expected to be generated by the accreting BH, as discussed in Sec.3.1. Here we consider an internally cold outflow with a mild to moderate Lorentz factor  $\Gamma \sim 10$  beamed into a solid angle  $\Omega$ . This outflow would produce EM emission in two ways. First, by bulk Comptonization of the disk photons, also known as Compton Drag (CD), and secondly by synchrotron emission, upon impacting the dense supernova remnant material.

Let us first consider the CD emission. The Comptonized spectrum can be easily calculated by boosting each photon's frequency by a factor  $\Gamma^2$  (Rybicki & Lightman 1986; Lazzati et al. 2000). In a steady-state scenario, like the one envisaged here, the bolometric luminosity is boosted by a factor  $L_{\text{bol,CD}} = \min[\tau_T, 1]L_{\text{bol,seed}}\Gamma^2$ , where  $\tau_T$  is the Thomson optical depth of the relativistic outflow and  $L_{\text{bol,seed}}$  is the luminosity of the seed photons, in our case the disk emission. The resulting spectra are shown in Figure 3 with a green line, under the assumption  $\tau_T \geq 1$ . While this assumption may not always be realized, we considered carrying out a full integration to be beyond the scope of this work, given that the CD emission is never the one matching the observations in the three considered transients. We also assumed  $\Gamma$  to be constant, while the outflow might be accelerating at the smallest distances. The green lines in Figure 3 should therefore be considered as an upper limit for the CD emission.

Finally, let us consider the emission from the jet itself, as it strikes the external medium driving relativistic shocks both into the external medium and into the jet itself (reverse shock). This emission component is analogous to what is observed in gamma-ray bursts (GRBs). The outflow propagates in the high density external medium of the SN ejecta,

$$n_{\text{SNR}} = \frac{3\zeta M_{\text{ej}}}{4\pi m_p d^3} = 10^{14} \frac{M_{\text{ej}}}{M_{\odot}} \frac{\zeta}{10^{-3}} \left( \frac{d}{1 \text{ AU}} \right)^{-3} \text{ cm}^{-3} \quad (20)$$

and therefore produces electromagnetic emission through its interaction with the external material, akin to the case of gamma-ray bursts in very high density media described in Wang et al. (2022) and Lazzati et al. (2022). In this regime the emission is predominantly driven by the repetitive shocks that the outflow shells produce hitting the external medium (Lazzati et al. 2022, 2023), rather than being produced as in the classic scenario in which shells hit each other first (the so-called internal shocks, Rees & Meszaros 1994). We used the semi-analytical code developed by Lazzati et al. (2022, 2023) to compute the synchrotron emission. The outflow was assumed to be made of 10 shells, with a total engine activity duration corresponding to the viscosity timescale of Eq. 11. Equipartition parameters  $\epsilon_e = 0.2$  and  $\epsilon_B = 0.01$  were adopted (e.g., Panaitescu & Kumar 2002). To best mimic the prompt emission of GRBs, the spectrum was assumed to be flat ( $F(\nu) \propto \nu^0$ ) between the self-absorption and peak frequencies. At higher frequencies, two slopes are shown, to encompass the variability seen in gamma-ray bursts:  $F(\nu) \propto \nu^{-1.5}$  is shown with a thick line, and  $F(\nu) \propto \nu^{-2.5}$  is shown with a thin line. This component is shown in Figure 3 with a red line. The three panels show the calculated spectra for the three considered transients. All parameter values are kept at their fiducial values, except the orbital separation  $d$  and the ejecta velocity  $v_{\text{ej}}$ , which are tuned to the individual transient values inferred from Figure 2. In the AT2018cow panel (right) the outflow emission components are shown with dashed lines since the accretion rate is comparable to the Eddington value (depending on  $\eta$ ) and the presence of a collimated outflow is therefore uncertain. For this specific case, therefore, we concur with the disk emission interpretation put forward by Migliori et al. (2024). In our model, however, the disk surrounds the companion BH and is not the same engine responsible for the FLBOT explosion. We also notice that a BH more massive than  $15 M_{\odot}$  would be required to make the disk emission consistent with the observed luminosity. Alternatively, the observed X-ray emission could be interpreted as due to the external shock, if a jet indeed forms at accretion rates comparable with the Eddington rate.

### 3.3. Opacity and emerging radiation

Once the EM radiation is produced, it needs to propagate through the SN ejecta. To compute the column density of material that the transient radiation needs to propagate through, we adopt the model developed for SN1987A (Chevalier & Soker 1989; Chevalier & Fransson 1992). This model is based on homologous expansion and is parameterized on the remnant mass and kinetic energy. It consists of a broken power-law, the break position propagating outward and smoothly connecting a shallow slope at low radii ( $\rho_{\text{in}} \propto r^{-m}t^{m-3}$ ) with a steep slope at large distances ( $\rho_{\text{out}} \propto r^{-n}t^{n-3}$ ). Following Chevalier & Fransson (1992) we set  $m = 1$  and  $n = 9$ . In our specific calculation we also set the velocity of the power-law break in the density profile to match the evaluated expansion speed for each of the three considered FBOTs, and we hold the ejecta mass fixed to a solar mass. To convert column densities to optical depths we use mean opacity values for solar metallicity gas. For the optical/NIR regime we adopt  $\kappa_{\text{O/NIR}} = 10^{-3} \text{ g/cm}^2$ , which is fairly typical for supernova explosion calculations (e.g., Ensmann & Woosley 1988; Woosley & Heger 2007). For the X-ray regime, instead, we consider a solar metallicity gas in which all the K-shell electrons for  $Z \geq 6$  are bound to their nuclei, which is relevant for gas temperatures of less than  $\sim 10^5 \text{ K}$ . This gives (e.g., Lazzati & Perna 2002)  $\kappa_{\text{X}} \simeq 200 \text{ g/cm}^2$ .

The resulting optical depths are shown in Figure 4, with colors differentiating the three transients. For each case, the figure shows several scenarios: solid lines are computed for the optical/NIR band, while dashed lines refer to the

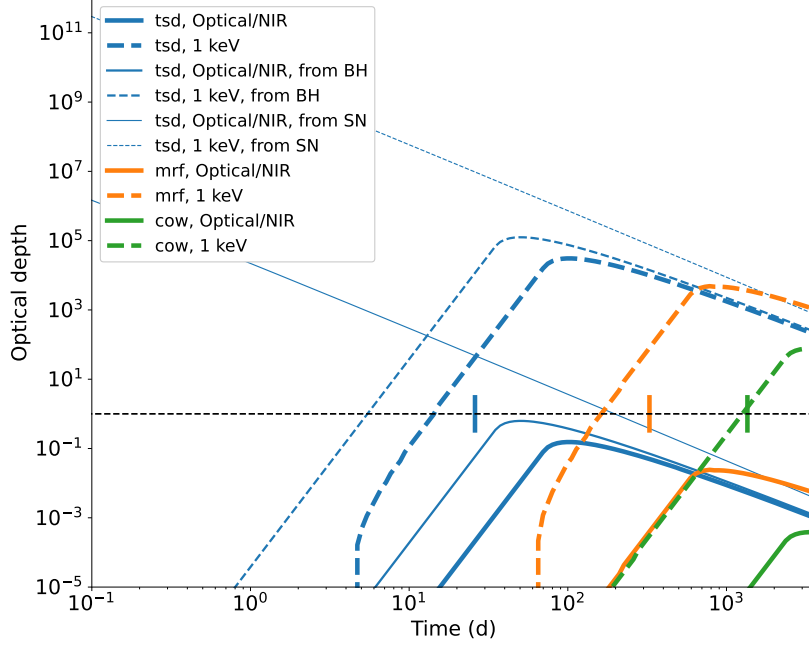


**Figure 4.** Opacity between the transient emission site and the observer at infinity for different scenarios in both the optical/NIR and X-ray bands (see Sect. 3.3 for more details).

X-ray band. For all the transients, thick lines refer to the opacity for a transient that is formed at the location of the external shock of the BH outflow. That is,

$$\tau = \kappa \int_{R_{\text{ES}}}^{\infty} \rho(r') dr', \quad (21)$$

where  $r'$  is the distance from the center of the BH and  $R_{\text{ES}}$  is computed via

$$M_c c^2 = \Gamma^2 \int_0^{R_{\text{ES}}} 4\pi \rho(r') r'^2 dr', \quad (22)$$

with  $\Gamma$  being the Lorentz factor of the outflow.

The trends of the thickest lines can be interpreted as follow. If there is no opacity, typically at early times, it is because the jet is able to propagate through and emerge from the remnant before triggering an external shock. At later time, the opacity increases because the amount of material at a radius that is larger than the location of the companion BH grows. Finally, at very late times, the remnant has become so big that the main effect is the dilution of the density, causing the opacity to then decrease. It is interesting to notice that the feature of an increasing and then decreasing optical depth is unique to this model and would potentially be a way to distinguish it from models in which the accretion responsible for the late time flares is onto the same engine that drove the FLBOT itself.

For the case of AT2022tsd, which is especially constraining due to its fast variability, we also show the opacity for radiation produced by the disk (or any other source) at the position of the BH. In this case,

$$\tau_{\text{BH}} = \kappa \int_0^{\infty} \rho(r') dr' \quad (23)$$

and we use a thinner line with respect to the one used for  $\tau$ . Notice how the opacity is larger at early times, since this radiation is produced at the location of the BH and not at the external shock radius<sup>2</sup>. Finally, again only for the case of AT2022tsd, we plot the optical depth that a transient originating from the exploding star would see. This is computed as

<sup>2</sup> Note that we do not include here a possible wind component discussed in Sect. 3.2, which would increase the opacity for any photon produced close to the BH.

$$\tau_{\text{SN}} = \kappa \int_{10^{10}\text{cm}}^{\infty} \rho(r) dr. \quad (24)$$

We notice that the physical lower limit is needed to avoid divergence ( $\rho(r) \propto (1/r)$  in this regime) and was chosen to represent the radius of a compact star. We also emphasize that this integral is over  $r$ , the distance from the center of the exploding SN, and not from the center of the BH as in Eq. 21 and 23. We notice that any transient originating at the radius of the exploding star will likely be diffused, at least for a year after the explosion, and would not display fast variability as seen in AT2022tsd after about one month.

Finally, short vertical lines of the corresponding color show the time at which EM activity was observed in the three considered FBOTs. We see that for the AT2022tsd case the remnant is thin at optical/NIR frequencies, for both the ES and disk emission. It is, instead, opaque in X-rays. For the case of AT2020mrf, Figure 4 shows that the remnant is thick in X-rays. This is at odds with the observation of variable X-ray emission from the source. It should be noted, however, that we have neglected the clumping in our opacity calculations, and photons might be able to propagate without diffusion through the thinner medium between clumps, if the covering fraction of clumps is less than unity. In addition, the X-ray flux from AT2020mrf is overproduced by the model with the fiducial ejecta mass  $M_{\text{ej}} = M_{\odot}$  (see central panel of Figure 3) and a lower ejecta mass would both decrease the opacity and improve the agreement in the predicted and observed flux. We notice, finally, that it is critical that the radiation is produced by the external shock (which is the case in the central panel of Figure 3). Radiation from the disk and from the exploding star would be subject to a much higher opacity that is unlikely to be reduced enough by geometrical considerations and/or by reducing the remnant mass. Finally, AT2018cow lies at  $\tau \sim 1$  in the X-ray band, and does not have an issue with diffusion.

#### 4. POPULATION MODELS

To determine the frequency of binary systems which match the conditions of our model, we run population synthesis calculations with the rapid binary population synthesis code COSMIC<sup>3</sup> (Breivik et al. 2020). As a baseline, we take a fiducial set of model assumptions that apply the default prescriptions in COSMIC for a population of  $5 \times 10^6$  binaries with metallicity  $Z = 0.8 Z_{\odot}$ . We initialize the population with primary masses  $M_1$  following Kroupa (2001), secondary masses sampled uniformly between  $[0.08 M_{\odot}, M_1]$ , and orbital periods and eccentricities following the distributions fit by Sana et al. (2012). The most important model assumptions for determining the properties of binaries hosting BHs with stripped-star companions are the BH formation mechanism (and its resulting natal kick) and the division between which systems undergo stable mass transfer or common envelop evolution when a star fills its Roche lobe. We assume that compact objects form using the ‘delayed’ prescription from Fryer et al. (2012) and that natal kicks are drawn from a Maxwellian distribution with  $\sigma = 265$  km/s where the natal kick is linearly reduced by the fallback fraction,  $f_b$  as defined by Fryer et al. (2012). We assume that the outcomes of Roche-overflow interactions are determined through critical mass ratios,  $q_c = M_{\text{donor}}/M_{\text{accretor}}$ , as defined by Neijssel et al. (2019) such that Roche-overflowing systems with  $q \geq q_c$  enter a common envelope (CE) and systems with  $q < q_c$  enter stable mass transfer (SMT). In the case of a CE, we assume that the orbital energy is used with perfect efficiency to eject the envelope ( $\alpha = 1$  in the  $\alpha - \lambda$  formalism van den Heuvel (1976)). For SMT, we assume that accretion is limited to 10 times the thermal rate  $\dot{M}_{\text{thermal}} = M_{\text{accretor}}/\tau_{\text{thermal}}$ . All mass that is not accreted is assumed to carry away the specific angular momentum of the accretor.

Figure 5 shows the orbital properties of binaries where a stripped-envelope SN occurs with BH companion for our fiducial model in black. COSMIC assumes that all Roche-overflow mass transfer circularizes the binary, thus all SNe occur in circular orbits. We find a significant population of stripped-envelope SNe with BH companions with  $a = 10 - 1000$  AU. These originate from systems which avoid Roche overflow and contain BHs with masses between  $12 - 18 M_{\odot}$  and pre-explosion masses between  $10 - 20 M_{\odot}$ . In orbits with  $a < 10$  AU the binary progenitors undergo Roche overflow which leads to lower BH and pre-explosion stripped star masses. These results suggest that transients from clumpy accretion onto a BH companion can occur on both short and long timescales in appreciable quantities (c.f. Figure 2.)

To test the sensitivity of our results to the binary evolution assumptions we made, we ran three model variations. First we assume BHs receive no natal kick at their formation, but do experience the symmetric kick due to instantaneous

<sup>3</sup> <https://cosmic-popsynth.github.io/>

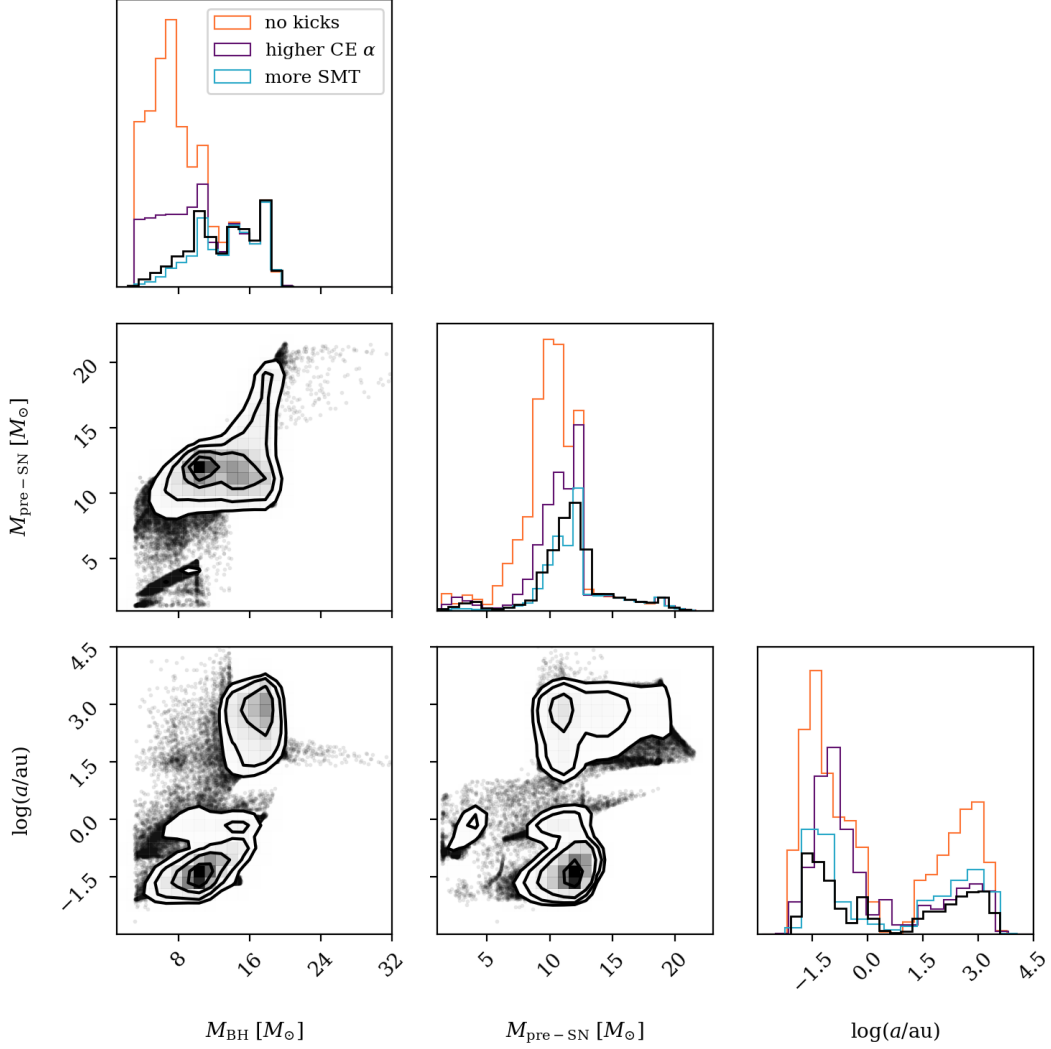


**Figure 5.** A corner plot showing the BH mass, pre-SN stripped star mass, and separation at the time of the SN for our fiducial model in black. Model variations are shown in the one-dimensional histograms with different colors.

mass loss in the orbit (Blaauw 1961). Next we consider the case where the CE ejection efficiency is raised to  $\alpha = 5$  such that some form of internal energy in the envelope can be used to unbind the envelope (Fragos et al. 2019). Finally, we increase the critical mass ratio for CE to  $q_c = 3$  consistent with Belczynski et al. (2008) which increases the number of systems which experience SMT.

Our model variations are shown in the one-dimensional histograms of Figure 5. Since each population was run with self-consistent initial conditions, the histogram heights accurately reflect the relative rates from each variation. The ‘more SMT’ variation produces the smallest change and leads to fewer close ( $a < 1$  AU) binaries. Both the ‘higher CE  $\alpha$ ’ and ‘no kicks’ variations lead to significantly more systems. In the CE variation, fewer binaries merge prior to the stripped-envelope SN because there is less shrinking in the orbit from both the mass transfer phase initiated by the BH progenitor and the mass transfer phase initiated by the stripped star progenitor relative to the fiducial model. This effect is more pronounced in close orbits since these binaries are more likely to survive a natal kick at the formation of the BH while wider systems will unbind due to the kick. Finally, when BHs receive no natal kick, the overall population size significantly increases both in close and wide systems. This effect is most pronounced in the BH mass panel where the lowest mass BHs are normally disrupted due to appreciable natal kicks under the fiducial model.

Finally, we note that for late-time transients ( $10 - 10^3$  days post SN), the binaries are wide enough to completely avoid Roche-overflow interactions. These systems are thus free from uncertainties which arise from mass transfer and are thus an exceptional window into BH formation and natal kicks. Conversely, future work to study the importance of ejecta interactions shortly after the supernova may shed important light on the uncertain binary interactions that produce stripped-envelope SNe in binaries with close BH companions.

## 5. DISCUSSION AND CONCLUSIONS

We have presented a model for late-time flaring and/or continuous emission in FLBOTs systems. Our model proposes a scenario in which the FLBOT is produced by an exploding massive compact star that is part of a close binary system with a companion BH. In most models discussed in the literature (e.g. Margutti et al. 2019; Yao et al. 2022; Migliori et al. 2024) the late emission is explained as activity from the same central engine that powered the FLBOT. In our model, instead, the late emission is due to material from the FLBOT ejecta that is accreted onto the companion BH. This has several advantages. Our model naturally accounts for the delay between the FLBOT and the late emission, due to the time it takes the ejecta to reach the orbit of the BH. In addition, since the BH is at the outer boundary of the ejecta, its emission suffers from much lower extinction and scattering, allowing for the engine variability timescale to be preserved. Finally, since the accretion is not driven by fallback and has an onset time that is different from the explosion time of the FLBOT, it is natural to observe fast variability like the one seen in AT2022tsd. To better understand this argument, consider the variability observed in GRB X-ray flares, which can be understood as due to late-time engine activity from a central engine accreting clumpy fallback material (Perna et al. 2006; Dall’Osso et al. 2017). Their variability timescale obeys  $\Delta t_{\text{flare}}/t_{\text{flare}} \sim 0.2$ , where  $\Delta t_{\text{flare}}$  is the flare duration and  $t_{\text{flare}}$  the delay of the X-ray flare photons from the GRB trigger (Chincarini et al. 2010). For AT2022tsd, minute duration flares were detected about a month after the FLBOT. These flares have therefore  $\Delta t_{\text{flare}}/t_{\text{flare}} \sim 10^{-5}$ , strikingly different from what observed in GRB X-ray flares. In the model presented here,  $t_{\text{flare}}$  would not be the time since the FLBOT but rather the time since the accreting clump has reached the companion BH, which can be as close as needed to the flare time. We consider the fast variability observed in AT2022tsd to be the principal reason for why a model like the one presented here is especially promising.

A better understanding of the physics involved would come from high-cadence panchromatic follow-up of future events. As shown in Figure 3, our model explains the fast variable optical emission as synchrotron from the shocked region between the BH outflow and the ejecta material. This is very broadband emission and simultaneous flares in a wide range of frequencies should be observable, provided that the remnant is thin at all frequencies. In addition, as the remnant grows in size, opacity is expected to increase and fast variability should disappear at late times. This is in contrast to models in which the central engine of the FLBOT and of the flares is the same, since opacity is expected to be monotonically declining in that geometry.

Should our model be supported by future data, searching for the predicted long-term emission (after a quiescent period) following a FLBOT explosion would be a powerful way to uncover the presence of a binary companion – and constrain its orbital separation. This is especially useful in light of the importance of these systems as gravitational wave sources. Additionally, a systematic analysis of the flare properties can provide valuable, independent constraints on the intrinsic properties of the SNR clumps. It should also be noted that this phenomenon may not be unique to FLBOTs. Any system in which an exploding star has a BH companion in a binary system will likely trigger accretion and electromagnetic emission (see also Fryer et al. 2014; Kimura et al. 2017b). Whether it would be detectable depends on the system geometry and dynamics, as discussed for the FLBOT case. Interestingly, our population synthesis modeling shows that binaries with the right separation should not be uncommon. However, unless the presence of a BH companion in the tens of AU range causes the stellar explosion to have the properties of an FLBOT, there is no reason not to expect fastly variable flares to follow more mundane core-collapse SN events.

As a final remark, the model that we discussed has some important simplifications that warrant further analysis. For example, it assumes a SN remnant with constant density and velocity, characterized by a large number of identical spherical clumps. In reality, it is more likely that the remnant is expanding in homologous fashion, with the fastest ejecta on the leading edge. The equations that we derived for a constant velocity show that the flares duration and luminosity depend on the ejecta velocity through the size of the accretion disk and the viscous timescale. If the clump geometry remains constant through the flow, the early flares would be expected to be longer and less luminous,

with increased activity at later time. In addition, clumps are likely to have a distribution in size, shape, and density contrast, favoring a diversity of flare properties that is not captured by our model in the simple version presented here.

#### ACKNOWLEDGMENTS

R.P. and D.L. thank the organizers of the FEET2024 workshop where this work was initiated. D.L. acknowledges support from NSF award AST-1907955. R.P. gratefully acknowledges support by NSF award AST-2006839.

#### REFERENCES

- Abellán, F. J., Indebetouw, R., Marcaide, J. M., et al. 2017, *ApJL*, 842, L24, doi: [10.3847/2041-8213/aa784c](https://doi.org/10.3847/2041-8213/aa784c)
- Belczynski, K., Kalogera, V., Rasio, F. A., et al. 2008, *ApJS*, 174, 223, doi: [10.1086/521026](https://doi.org/10.1086/521026)
- Blaauw, A. 1961, *BAN*, 15, 265
- Blandford, R. D., & Begelman, M. C. 1999, *MNRAS*, 303, L1, doi: [10.1046/j.1365-8711.1999.02358.x](https://doi.org/10.1046/j.1365-8711.1999.02358.x)
- Blandford, R. D., & Znajek, R. L. 1977, *MNRAS*, 179, 433, doi: [10.1093/mnras/179.3.433](https://doi.org/10.1093/mnras/179.3.433)
- Breivik, K., Coughlin, S., Zevin, M., et al. 2020, *ApJ*, 898, 71, doi: [10.3847/1538-4357/ab9d85](https://doi.org/10.3847/1538-4357/ab9d85)
- Byrne, R. A., & Fraser, M. 2022, *MNRAS*, 514, 1188, doi: [10.1093/mnras/stac1308](https://doi.org/10.1093/mnras/stac1308)
- Chen, Y., Drout, M. R., Piro, A. L., et al. 2023, *ApJ*, 955, 43, doi: [10.3847/1538-4357/ace964](https://doi.org/10.3847/1538-4357/ace964)
- Chevalier, R. A., & Fransson, C. 1992, *ApJ*, 395, 540, doi: [10.1086/171674](https://doi.org/10.1086/171674)
- Chevalier, R. A., & Soker, N. 1989, *ApJ*, 341, 867, doi: [10.1086/167545](https://doi.org/10.1086/167545)
- Chincarini, G., Mao, J., Margutti, R., et al. 2010, *MNRAS*, 406, 2113, doi: [10.1111/j.1365-2966.2010.17037.x](https://doi.org/10.1111/j.1365-2966.2010.17037.x)
- Dall’Osso, S., Perna, R., Tanaka, T. L., & Margutti, R. 2017, *MNRAS*, 464, 4399, doi: [10.1093/mnras/stw2695](https://doi.org/10.1093/mnras/stw2695)
- de Val-Borro, M., Karovska, M., & Sasselov, D. 2009, *ApJ*, 700, 1148, doi: [10.1088/0004-637X/700/2/1148](https://doi.org/10.1088/0004-637X/700/2/1148)
- Dessart, L., Hillier, D. J., & Wilk, K. D. 2018, *A&A*, 619, A30, doi: [10.1051/0004-6361/201833278](https://doi.org/10.1051/0004-6361/201833278)
- Drout, M. R., Chornock, R., Soderberg, A. M., et al. 2014, *ApJ*, 794, 23, doi: [10.1088/0004-637X/794/1/23](https://doi.org/10.1088/0004-637X/794/1/23)
- Edgar, R. 2004, *NewAR*, 48, 843, doi: [10.1016/j.newar.2004.06.001](https://doi.org/10.1016/j.newar.2004.06.001)
- Ensmann, L. M., & Woosley, S. E. 1988, *ApJ*, 333, 754, doi: [10.1086/166785](https://doi.org/10.1086/166785)
- Fabrika, S. 2004, *Astrophys. Space Phys. Res.*, 12, 1, doi: [10.48550/arXiv.astro-ph/0603390](https://doi.org/10.48550/arXiv.astro-ph/0603390)
- Fragos, T., Andrews, J. J., Ramirez-Ruiz, E., et al. 2019, *ApJL*, 883, L45, doi: [10.3847/2041-8213/ab40d1](https://doi.org/10.3847/2041-8213/ab40d1)
- Fransson, C., & Chevalier, R. A. 1989, *ApJ*, 343, 323, doi: [10.1086/167707](https://doi.org/10.1086/167707)
- Fryer, C. L., Belczynski, K., Wiktorowicz, G., et al. 2012, *ApJ*, 749, 91, doi: [10.1088/0004-637X/749/1/91](https://doi.org/10.1088/0004-637X/749/1/91)
- Fryer, C. L., Rueda, J. A., & Ruffini, R. 2014, *ApJL*, 793, L36, doi: [10.1088/2041-8205/793/2/L36](https://doi.org/10.1088/2041-8205/793/2/L36)
- Gottlieb, O., Tchekhovskoy, A., & Margutti, R. 2022, *MNRAS*, 513, 3810, doi: [10.1093/mnras/stac910](https://doi.org/10.1093/mnras/stac910)
- Ho, A. Y. Q., Perley, D. A., Chen, P., et al. 2023, *Nature*, 623, 927, doi: [10.1038/s41586-023-06673-6](https://doi.org/10.1038/s41586-023-06673-6)
- Huarte-Espinosa, M., Carroll-Nellenback, J., Nordhaus, J., Frank, A., & Blackman, E. G. 2013, *MNRAS*, 433, 295, doi: [10.1093/mnras/stt725](https://doi.org/10.1093/mnras/stt725)
- Jerkstrand, A., Fransson, C., & Kozma, C. 2011, *A&A*, 530, A45, doi: [10.1051/0004-6361/201015937](https://doi.org/10.1051/0004-6361/201015937)
- Jiang, Y.-F., Stone, J. M., & Davis, S. W. 2014, *ApJ*, 796, 106, doi: [10.1088/0004-637X/796/2/106](https://doi.org/10.1088/0004-637X/796/2/106)
- Kawaguchi, T. 2003, *ApJ*, 593, 69, doi: [10.1086/376404](https://doi.org/10.1086/376404)
- Kimura, S. S., Murase, K., & Mészáros, P. 2017a, *ApJ*, 851, 53, doi: [10.3847/1538-4357/aa988b](https://doi.org/10.3847/1538-4357/aa988b)
- . 2017b, *ApJ*, 851, 53, doi: [10.3847/1538-4357/aa988b](https://doi.org/10.3847/1538-4357/aa988b)
- Kochanek, C. S. 2021, *MNRAS*, 507, 5832, doi: [10.1093/mnras/stab2483](https://doi.org/10.1093/mnras/stab2483)
- Kochanek, C. S., Auchettl, K., & Belczynski, K. 2019, *MNRAS*, 485, 5394, doi: [10.1093/mnras/stz717](https://doi.org/10.1093/mnras/stz717)
- Kroupa, P. 2001, *MNRAS*, 322, 231, doi: [10.1046/j.1365-8711.2001.04022.x](https://doi.org/10.1046/j.1365-8711.2001.04022.x)
- Kuin, N. P. M., Wu, K., Oates, S., et al. 2019, *MNRAS*, 487, 2505, doi: [10.1093/mnras/stz053](https://doi.org/10.1093/mnras/stz053)
- Lazzati, D., Ghisellini, G., Celotti, A., & Rees, M. J. 2000, *ApJL*, 529, L17, doi: [10.1086/312452](https://doi.org/10.1086/312452)
- Lazzati, D., Morsony, B. J., Blackwell, C. H., & Begelman, M. C. 2012, *ApJ*, 750, 68, doi: [10.1088/0004-637X/750/1/68](https://doi.org/10.1088/0004-637X/750/1/68)
- Lazzati, D., & Perna, R. 2002, *MNRAS*, 330, 383, doi: [10.1046/j.1365-8711.2002.05064.x](https://doi.org/10.1046/j.1365-8711.2002.05064.x)
- Lazzati, D., Perna, R., Gompertz, B. P., & Levan, A. J. 2023, *ApJL*, 950, L20, doi: [10.3847/2041-8213/acd18c](https://doi.org/10.3847/2041-8213/acd18c)
- Lazzati, D., Soares, G., & Perna, R. 2022, *ApJL*, 938, L18, doi: [10.3847/2041-8213/ac98ad](https://doi.org/10.3847/2041-8213/ac98ad)
- Leung, S.-C., Fuller, J., & Nomoto, K. 2021, *ApJ*, 915, 80, doi: [10.3847/1538-4357/abfcbe](https://doi.org/10.3847/1538-4357/abfcbe)
- Lyutikov, M. 2022, *MNRAS*, 515, 2293, doi: [10.1093/mnras/stac1717](https://doi.org/10.1093/mnras/stac1717)

- Margutti, R., Metzger, B. D., Chornock, R., et al. 2019, *ApJ*, 872, 18, doi: [10.3847/1538-4357/aafa01](https://doi.org/10.3847/1538-4357/aafa01)
- Metzger, B. D. 2022, *ApJ*, 932, 84, doi: [10.3847/1538-4357/ac6d59](https://doi.org/10.3847/1538-4357/ac6d59)
- Migliori, G., Margutti, R., Metzger, B. D., et al. 2024, *ApJL*, 963, L24, doi: [10.3847/2041-8213/ad2764](https://doi.org/10.3847/2041-8213/ad2764)
- Mohan, P., An, T., & Yang, J. 2020, *ApJL*, 888, L24, doi: [10.3847/2041-8213/ab64d1](https://doi.org/10.3847/2041-8213/ab64d1)
- Neijssel, C. J., Vigna-Gómez, A., Stevenson, S., et al. 2019, *MNRAS*, 490, 3740, doi: [10.1093/mnras/stz2840](https://doi.org/10.1093/mnras/stz2840)
- Neustadt, J. M. M., Kochanek, C. S., Stanek, K. Z., et al. 2021, *MNRAS*, 508, 516, doi: [10.1093/mnras/stab2605](https://doi.org/10.1093/mnras/stab2605)
- Panaiteescu, A., & Kumar, P. 2002, *ApJ*, 571, 779, doi: [10.1086/340094](https://doi.org/10.1086/340094)
- Parfrey, K., Philippov, A., & Cerutti, B. 2019, *PhRvL*, 122, 035101, doi: [10.1103/PhysRevLett.122.035101](https://doi.org/10.1103/PhysRevLett.122.035101)
- Pasham, D. R., Ho, W. C. G., Alston, W., et al. 2021, *Nature Astronomy*, 6, 249, doi: [10.1038/s41550-021-01524-8](https://doi.org/10.1038/s41550-021-01524-8)
- Pellegrino, C., Howell, D. A., Vinkó, J., et al. 2022, *ApJ*, 926, 125, doi: [10.3847/1538-4357/ac3e63](https://doi.org/10.3847/1538-4357/ac3e63)
- Perley, D. A., Mazzali, P. A., Yan, L., et al. 2019, *MNRAS*, 484, 1031, doi: [10.1093/mnras/sty3420](https://doi.org/10.1093/mnras/sty3420)
- Perna, R., Armitage, P. J., & Zhang, B. 2006, *ApJL*, 636, L29, doi: [10.1086/499775](https://doi.org/10.1086/499775)
- Perna, R., Duffell, P., Cantiello, M., & MacFadyen, A. I. 2014, *ApJ*, 781, 119, doi: [10.1088/0004-637X/781/2/119](https://doi.org/10.1088/0004-637X/781/2/119)
- Piro, A. L., & Lu, W. 2020, *ApJ*, 894, 2, doi: [10.3847/1538-4357/ab83f6](https://doi.org/10.3847/1538-4357/ab83f6)
- Prentice, S. J., Maguire, K., Smartt, S. J., et al. 2018, *ApJL*, 865, L3, doi: [10.3847/2041-8213/aadd90](https://doi.org/10.3847/2041-8213/aadd90)
- Qian, Q., Fendt, C., & Vourellis, C. 2018, *ApJ*, 859, 28, doi: [10.3847/1538-4357/aabd36](https://doi.org/10.3847/1538-4357/aabd36)
- Quataert, E., Lecoanet, D., & Coughlin, E. R. 2019, *MNRAS*, 485, L83, doi: [10.1093/mnrasl/slz031](https://doi.org/10.1093/mnrasl/slz031)
- Rees, M. J., & Meszaros, P. 1994, *ApJL*, 430, L93, doi: [10.1086/187446](https://doi.org/10.1086/187446)
- Rybicki, G. B., & Lightman, A. P. 1986, *Radiative Processes in Astrophysics*
- Sana, H., de Mink, S. E., de Koter, A., et al. 2012, *Science*, 337, 444, doi: [10.1126/science.1223344](https://doi.org/10.1126/science.1223344)
- Shakura, N. I., & Sunyaev, R. A. 1973, *A&A*, 24, 337
- Smartt, S. J., Clark, P., Smith, K. W., et al. 2018, *The Astronomer's Telegram*, 11727, 1
- Takeuchi, S., Ohsuga, K., & Mineshige, S. 2013, *PASJ*, 65, 88, doi: [10.1093/pasj/65.4.88](https://doi.org/10.1093/pasj/65.4.88)
- Tchekhovskoy, A., Narayan, R., & McKinney, J. C. 2011, *MNRAS*, 418, L79, doi: [10.1111/j.1745-3933.2011.01147.x](https://doi.org/10.1111/j.1745-3933.2011.01147.x)
- van den Heuvel, E. P. J. 1976, in *Structure and Evolution of Close Binary Systems*, ed. P. Eggleton, S. Mitton, & J. Whelan, Vol. 73, 35
- Wang, C.-Y. 2001, PhD thesis, University of Virginia
- Wang, C.-Y., & Chevalier, R. A. 2002, *ApJ*, 574, 155, doi: [10.1086/340795](https://doi.org/10.1086/340795)
- Wang, Y.-H., Lazzati, D., & Perna, R. 2022, *MNRAS*, 516, 5935, doi: [10.1093/mnras/stac1968](https://doi.org/10.1093/mnras/stac1968)
- Woosley, S. E., & Heger, A. 2007, *PhR*, 442, 269, doi: [10.1016/j.physrep.2007.02.009](https://doi.org/10.1016/j.physrep.2007.02.009)
- Yao, Y., Ho, A. Y. Q., Medvedev, P., et al. 2022, *ApJ*, 934, 104, doi: [10.3847/1538-4357/ac7a41](https://doi.org/10.3847/1538-4357/ac7a41)
- Zhang, W., Woosley, S. E., & Heger, A. 2008, *ApJ*, 679, 639, doi: [10.1086/526404](https://doi.org/10.1086/526404)